Constraints on the active tectonics of the Friuli/NW Slovenia area from CGPS measurements and three-dimensional kinematic modeling

M. Bechtold,[1,2] M. Battaglia,[3] D. C. Tanner,[1,4] and D. Zuliani[5]

Received 17 February 2008; revised 5 November 2008; accepted 7 January 2009; published 26 March 2009.

[1] We use site velocities from continuous GPS (CGPS) observations and kinematic modeling to investigate the active tectonics of the Friuli/NW Slovenia area. Data from 42 CGPS stations around the Adriatic indicate an oblique collision, with southern Friuli moving NNW toward northern Friuli at the relative speed of 1.6 to 2.2 mm/a. We investigate the active tectonics using 3DMove, a three-dimensional kinematic model tool. The model consists of one indenter-shaped fault plane that approximates the Adriatic plate boundary. Using the ''fault-parallel flow'' deformation algorithm, we move the hanging wall along the fault plane in the direction indicated by the GPS velocities. The resulting strain field is used for structural interpretation. We identify a pattern of coincident strain maxima and high vorticity that correlates well with groups of hypocenters of major earthquakes (including their aftershocks) and indicates the orientation of secondary, active faults. The pattern reveals structures both parallel and perpendicular to the strike of the primary fault. In the eastern sector, which shows more complex tectonics, these two sets of faults probably form an interacting strike-slip system.

Citation: Bechtold, M., M. Battaglia, D. C. Tanner, and D. Zuliani (2009), Constraints on the active tectonics of the Friuli/NW Slovenia area from CGPS measurements and three-dimensional kinematic modeling, *J. Geophys. Res.*, *114*, B03408, doi:10.1029/2008JB005638.

1. Introduction

[2] The eastern southern Alps region is one of the most seismically active regions of Italy. Because of the high population density and the density of industrial settlements, the region is highly vulnerable to earthquakes. Infrequent $M > 6$ earthquakes, together with frequent smaller earthquakes, characterize the seismic hazard in the Friuli/NW Slovenia area [*Bressan et al.*, 2003]. The reason for these ground motions, emphasized by the 1976 Friuli seismic sequence, is the independent anticlockwise rotation of the Adriatic microplate within the Africa-Eurasia collision zone [e.g., *Anderson and Jackson*, 1987; *Battaglia et al.*, 2004]. Results of the recently performed seismic TRANSALP profile in the Eastern Alps are consistent with deep underthrusting and wedge indentation of the Adriatic lithosphere under the southern margin of the Eastern Alps thrust-and-fold belt [*Castellarin et al.*, 2006]. The ongoing N–S to NW–SE compression [e.g., *Bressan et al.*, 1998; *D'Agostino et al.*, 2005], with faulting mainly along NE–SW to NW–SE trending thrusts and the deformation of the Quaternary deposits of the Friulian Plain [*Galadini et al.*, 2005] indicate that the eastern southern Alps can be presently described as a south verging, foreland-propagating thrust system. According to *D'Agostino et al.* [2005], the motion of Adria is entirely absorbed in the southern Alps through thrusting and crustal thickening, with very little or no motion transferred to the north.

[3] Knowledge of the related seismogenic sources is sparse [e.g., *Bressan et al.*, 1998, 2003; *Slejko et al.*, 1999; *Poli et al.*, 2002; *Poli and Renner*, 2004; *Galadini et al.*, 2005; DISS Working Group, Database of Individual Seismogenic Sources (DISS), version 3: A compilation of potential sources for earthquakes larger than M 5.5 in Italy and surrounding areas, 2006, available at http://www.ingv.it/DISS/, hereinafter referred to as DISS Working Group, database, 2006] (see Figure 1). The recent tectonic activity is suspected to be related to motion on blind thrusts, some of them covered by the Quaternary deposits of the Friulian Plain. A major controlling factor is ascribed to the complex paleofault system of the area. Several Cenozoic compressional tectonic phases related to the Alpine Orogeny caused SW–NE trending faults in the western, E–W trending faults in the central, and SE–NW trending faults in the eastern sector [*Bressan et al.*, 1998, 2003; *Galadini*

[1]Department of Structural Geology and Geodynamics, Geoscience Center, Göttingen, Germany.
[2]Institute of Chemistry and Dynamics of the Geosphere, Institute Agrosphere, Research Centre Juelich, Juelich, Germany.
[3]Department of Earth Sciences, University of Rome I ''La Sapienza,'' Rome, Italy.
[4]Now at the Leibniz Institute for Applied Geosciences, Hannover, Germany.
[5]Centro Ricerche Sismologiche, Udine, Italy.

0148-0227/09/2008JB005638$09.00

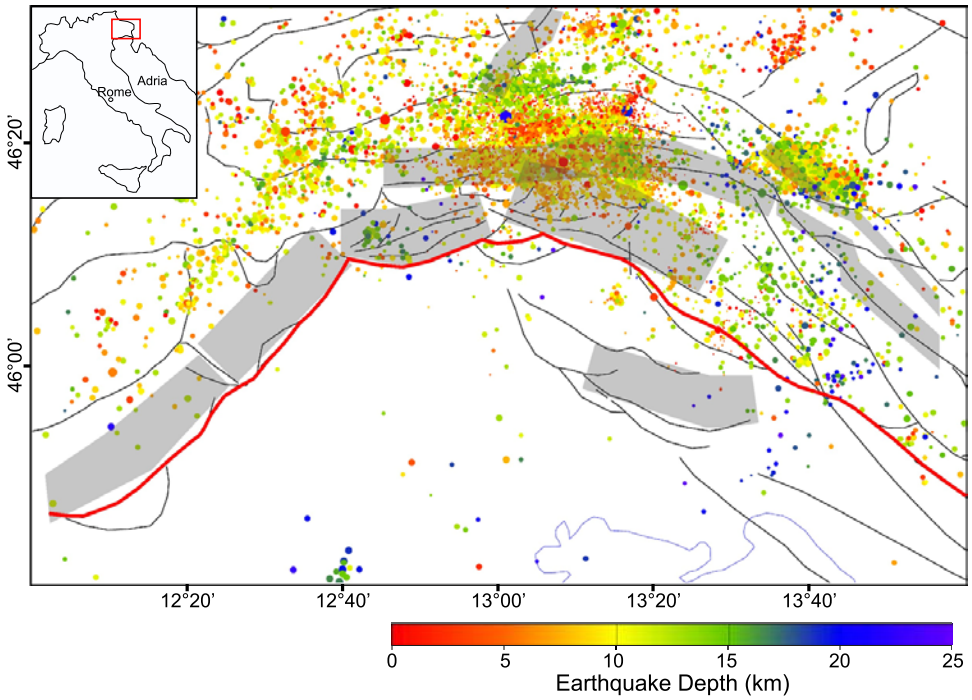

Figure 1. Seismicity distribution in Friuli. Gray polygons represent proposed seismogenic sources after DISS Working Group (database, 2006). Seismicity distribution is shown as dots scaled to magnitude and colored by depth. The structural map of *Galadini et al.* [2005] (with permission) is also shown. The red line represents the trace of the modeled thrust fault. Inset shows the position of the study area in Italy.

et al., 2005]. The seismicity distribution observed since 1977 cannot only be related to one active thrust front (Figure 1). Beside the proposed active faults, the area is probably characterized by other, as yet not recognized, active structures.

[4] We address the complex active tectonics of the Friuli (Italy)/NW Slovenia area with an approach that combines GPS site velocities and kinematic modeling. In the first part, we present our GPS processing procedure and the resulting velocity field. In the second part, we present the modeling tool 3DMove and the data basis of our model. To support our data basis, we discuss the sensitivity of the resulting strain field to movement direction and fault plane selection. Finally, we discuss the results and compare them with observed seismicity.

2. Friuli GPS Velocity Field

[5] Since 2002, high-precision geodesy, i.e., the Friuli Regional Deformation Network (FReDNet) consisting of eight continuously operating GPS receivers, monitors the movements of the crust in the Friuli area and provides an important tool for characterizing crustal deformation processes [*Battaglia et al.*, 2004; *D'Agostino et al.*, 2005]. In our work, we update and improve upon earlier results by *D'Agostino et al.* [2005]. In particular, we include all the eight stations of the FReDNet network, and we use a complete different approach to process the CGPS data and estimate the velocities uncertainties. This allows us to produce a set of solutions completely independent from earlier results. Furthermore, thanks to the increasing number of CGPS sites existing in the public domain, we included in our solution twice the number of sites used by *D'Agostino et al.* [2005]. To determine the crustal velocity field of this area, we consistently analyzed data from 42 GPS stations around the Adriatic region. All data used in this analysis are in the public domain (http://www.crs.inogs.it/frednet). The GPS data were processed applying a three-step approach, e.g., the method of *Feigl et al.* [1993], using the GAMIT/GLOBK GPS analysis package (http://www-gpsg.mit.edu/~simon/gtgk/index.htm).

[6] To aid orbit determination and to strengthen the reference frame for the velocity solution, we included additional sites from the international GPS Service and EUREF networks as loosely constrained solutions provided by the Scripps Orbit and Permanent Array Center (SOPAC) [*McClusky et al.*, 2000; *Herring*, 2003a]. Ten stations, present both in our regional analysis and in the global analysis by SOPAC, provide a link between the two solutions. In the end, our solution includes data spanning 4.5 years from 250 stations. All eight continuous operating GPS stations of FReDNet present at least 2.5 years of data (Table 1), the minimum time span to reliably determine crustal velocities [*Blewitt and Lavallée*, 2002].

[7] Since the expected velocities of the GPS stations in the Friuli area are in the range of few millimeters per year, it was very important to properly determine the uncertainties of the velocity estimates. We performed an error estimation that accounts for both white and random walk noise [e.g., *McClusky et al.*, 2000]. The combination of daily quasi-observations into weekly, monthly or annual averages is a method to account for white noise [*McClusky et al.*, 2000; R. W. King and T. A. Herring, personal communication, 2006]. R. W. King and T. A. Herring propose that monthly

Table 1. Site Velocities and Standard Deviations of the N, E, and U Components of the FReDNet Stations in the European Reference Frame[a]

ID	Station	Longitude	Latitude	Time Span (years)	Site Velocities		
					N	E	U
ACOM	Monte Acomizza	13.515	46.548	3.3	0.66 ± 0.22	−0.37 ± 0.22	−0.48 ± 1.23
AFAL	Alpe Faloria	12.175	46.527	3.4	0.87 ± 0.21	−0.44 ± 1.15	0.55 ± 1.36
CANV	Caneva	12.435	46.008	2.5	2.83 ± 0.69	−2.04 ± 0.41	−0.41 ± 1.73
MDEA	Colle di Medea	13.436	45.924	3.8	2.25 ± 0.25	−1.37 ± 0.21	−2.26 ± 1.18
MPRA	Mont di Prat	12.988	46.241	4.2	1.76 ± 0.24	−0.74 ± 0.25	−1.04 ± 1.18
UDIN	Udine	13.253	46.037	3.9	3.23 ± 0.49	−0.24 ± 0.50	−7.95 ± 1.55
TRIE	Trieste	13.764	45.710	3.7	2.30 ± 0.24	−0.84 ± 0.34	2.17 ± 1.12
ZOUF	Zouf Plan	12.974	46.557	4.4	1.05 ± 0.20	−0.39 ± 0.28	−2.49 ± 1.13

[a]Site velocities are in mm/a. For the European reference frame, see *Altamimi et al.* [2002].

combinations provide sufficient observations for a good statistics on the residuals about the linear trends. White noise was estimated by manually adjusting the scaling on the quasi-observations (h files) such that the prefit χ^2 is close to 1. A prefit χ^2 that is close to 1 results in one-σ data uncertainties that are equal to the average scatter of the data residuals about the solution [*McClusky et al.*, 2000]. The data scatter provides an unbiased estimate of the uncertainties if the error spectrum is white and the data are spatially and temporally sampled homogeneously. The random walk component was estimated separately for each station using the "realistic sigma" algorithm of *Herring* [2003b] [e.g., *Reilinger et al.*, 2006]. The average of all estimated random walk components is 0.8 mm/$\sqrt{a}$ in the horizontal and 6 mm/$\sqrt{a}$ in the vertical (Table 2). The stable Eurasian plate by *Altamimi et al.* [2002] provides the reference frame for the velocity estimation. All details on the complete GPS processing procedure are documented by *Bechtold* [2007].

[8] The Friuli crustal velocity field illustrates the specific tectonic position of the Friuli area situated between the "stable" sites of the Alps and the NNW moving sites of northern Adria (Figure 2 and Table 1). The results indicate that the FReDNet GPS sites can be divided into three groups: (1) AFAL, ACOM, and ZOUF (northern Friuli) moving north to NNW with 0.8 to 1.1 mm/a; (2) CANV, MDEA, TRIE, and UDIN (southern Friuli) moving north to NNW with 2.5 to 3.5 mm/a; and (3) MPRA moving NNW with 1.9 mm/a, representing an intermediate position. The angle of collision of southern Friuli with respect to northern Friuli can be inferred from a solution stabilized for northern Friuli. This suggests a NNW movement of about 330°. The velocity field indicates shortening within the Friuli area of about 1.6 to 2.2 mm/a. This value can be compared with that determined by *D'Agostino et al.* [2005] of 2.0 ± 0.2 mm. The shortening rate is consistent with geomorphologic studies along the Montello Thrust, which indicate a NW directed shortening at a rate of ~2 mm/a [*Benedetti et al.*, 2000]. The uncertainties in the vertical component are too large for reliable conclusions (Table 1). The velocity field is consistent with previously published GPS site velocities [*D'Agostino et al.*, 2005] but presents more details in the specific study area. In the last years several GPS velocity fields of the Adriatic region have been published [e.g., *Battaglia et al.*, 2004; *Serpelloni et al.*, 2007]. In the published results the movement direction and velocity of northern Adria relative to stable Eurasia ranges from NNW to NNE at 2.5 mm/a to 4.5 mm/a. Variations are mainly caused by different lengths of time series and by using different sites as reference for stable Eurasia. *Grenerczy et al.* [2005] observed a 2–3 mm/a of N–S Adria-Eurasia convergence that is taken up by contradiction across a narrow (70 km) zone in the Eastern Alps resulting in a net 30 ppb/a contractional strain rate. A shortening of 2–3 mm/a was also proposed by *D'Agostino et al.* [2005] and *Caporali et al.* [2008]. Most GPS studies have not included FReDNet stations (besides TRIE) and the closest stations were UPAD, MEDI, BOZI, and MALJ. One exception is the work of *D'Agostino et al.* [2005], who presented the first GPS site velocities of the stations TRIE, MDEA, UDIN, MPRA and ZOUF. Using 1–1.5 years longer time series and more stations our GPS processing results refine previous Friuli GPS velocity fields by giving a better spatial resolution and reduction of the uncertainties, and by providing the first complete processing of FReDNet.

3. Kinematic Model

[9] We use the information obtained from the velocity field of the GPS processing to constrain a three-dimensional, kinematic model. Kinematic modeling is a well-established tool for structural restoration and is applied in the oil and gas, mining, and nuclear waste industries to validate and analyze 3-D models (Figure 3). The indenter tectonics and the NNW oriented, oblique collision are three-dimensional interactions and therefore, the application of a 3-D model space is necessary. The philosophy of our modeling approach is to infer unknown structures due to the movement along primary, known structures (Figure 3).

[10] The kinematic modeling was performed using the software package 3DMove (http://www.mve.com/3DMove/

Table 2. Site-Specific Random Walk Components[a]

	Random Walk Components (mm/$\sqrt{a}$)		
	N	E	U
ACOM	0.11	0.11	3.93
AFAL	0.08	4.18	4.74
CANV	1.05	0.33	5.54
MDEA	0.17	0.10	4.22
MPRA	0.17	0.20	4.78
TRIE	0.16	0.36	3.84
UDIN	0.83	0.87	7.89
ZOUF	0.12	0.28	4.63
Average	0.34	0.80	4.95

[a]Site-specific random walk components are estimated by the "realistic sigma" algorithm [*Herring*, 2003b]; random walk for each component (N, E, and U) of the FReDNet stations are given.

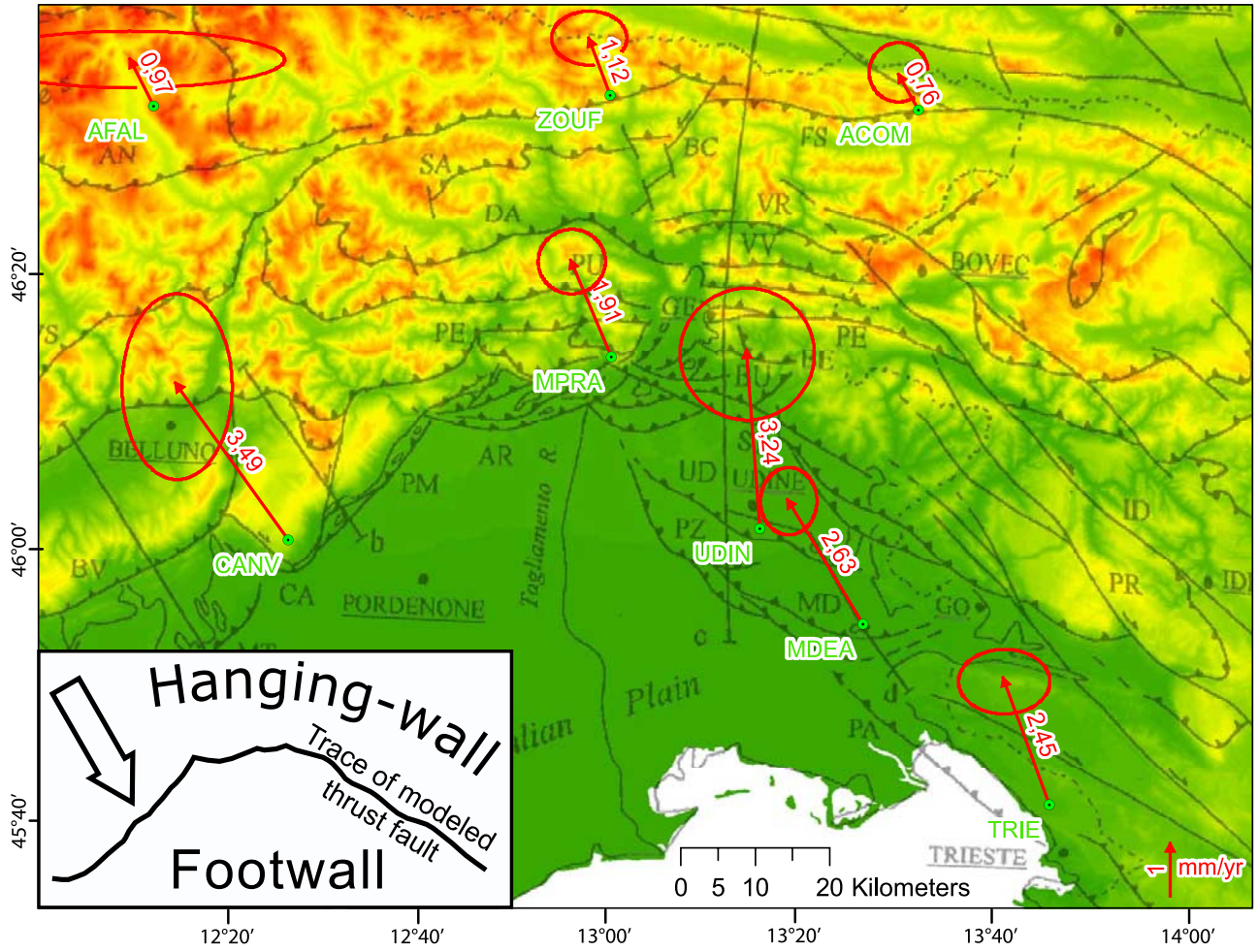

Figure 2. Friuli deformation velocity field relative to stable Eurasia. The velocities are represented by vectors (in mm/a). The error ellipses indicate the 95% confidence level (2 standard deviations). Structural map is after *Galadini et al.* [2005] (with permission). DEM from the Shuttle Radar Topography Mission SRTM (http://www2.jpl.nasa.gov/srtm). The movement direction of the hanging wall relative to the footwall needed for the kinematic model is shown in the inset (SSE at 150°).

3dmove.html). First, we used all available information (structural maps, cross sections, seismicity distribution, GPS velocity field and DEM) to build one indenter-shaped fault plane 200 km long and 20 km deep that approximates the Adriatic plate boundary, i.e., the active front of the foreland-propagating thrust system.

3.1. Fault Plane Construction

[11] The first challenge was the construction of a continuous fault plane, taking into account all available information on active structures: the velocity field, proposed seismogenic sources, structural maps, cross sections (see below), seismicity and DEM.

[12] There is little doubt that the thrusts bordering the Venetian and Friulian Plains are the most recently active structures [e.g., *Benedetti et al.*, 2000; *Galadini et al.*, 2005]. In the western and central sector, this assumption corresponds well with the proposed seismogenic sources. For the eastern sector, we extended the fault plane along proposed fault traces that border the Friulian Plain. Although the fault

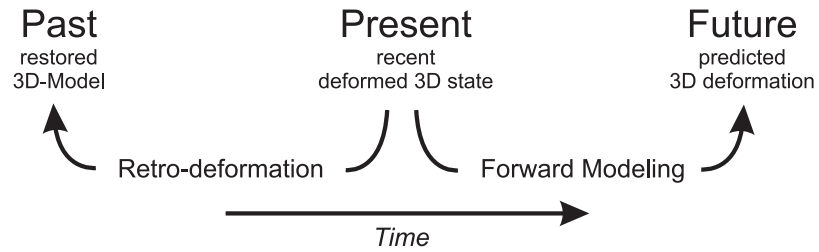

Figure 3. Kinematic modeling can be used for both structural restoration (retrodeformation) as well as to predict future deformation patterns (forward modeling).

traces used for this sector are not related to proposed seismogenic sources, they fulfill two important criteria: they have location (1) south of the seismicity belt and (2) north of the velocity solutions of UDIN, MDEA and TRIE stations (all with velocities appropriate to the Adriatic microplate).

[13] For the digitalization of the superficial fault traces, we preferred the structural map of *Galadini et al.* [2005] (see Figure 4), because they also provided two cross sections used in the fault plane construction. The available four cross sections were used to infer the trace of the fault at depth. Unfortunately, they do not indicate whether the cross sections have been retrodeformed and quantitatively balanced or not. The four cross sections are (numbers refer to Figure 4):

[14] 1. Cross section 1 [*Galadini et al.*, 2005] is a NW–SE cross section, which crosses the Montello Thrust Fault and is based on reflection seismic data published by *Fantoni et al.* [2001] and structural data.

[15] 2. Cross section 2 [*Galadini et al.*, 2005] is a NW–SE cross section. This section crosses the Polcenigo-Maniago Thrust Fault and is derived from superficial geologic and structural as well as subcrop information (unpublished Eni/Agip reflection seismic surveys).

[16] 3. Cross section 3 [*Carulli and Ponton*, 1992] is a N–S cross section. This section interprets the geometry of the planes of deep thrusts in the central sector of Friuli and is based on published, as well unpublished, geologic, magnetic, and seismologic data. Three main E–W striking, north dipping structural systems of Neogene age have been described: the Northern Valsugana System, the High Tagliamento System, and the Piedmont System. The last is supposed to be the recently active, foreland-propagating front. It is situated in high proximity to the Dinaric system.

[17] 4. Cross section 4 [*Poli et al.*, 2002] is a N–S geologic section. Southern sector coincides with the geologic cross section of *Peruzza et al.* [2002]. The data set for the northern sector is mainly based on bibliographic data, while the southern one is based on new field geologic observations, the revised stratigraphy resulting from AGIP oil wells in eastern Friuli, and on the reanalysis of AGIP seismic lines crossing the Friulian Plain.

[18] We georeferenced both the structural map and the cross sections using ArcGIS. To provide the surface-building algorithms of 3DMove more constraints, we constructed subcrop fault strike maps. We fitted them to the trace of the fault at depth. Each set of subcrop fault strike maps was connected individually using the Spline algorithm. The three resultant surfaces were linked using the Tessellation algorithm. Using the Create Mid algorithm a new surface was created with smoothed sharp edges and a regular wire triangular frame, a structure that is desirable for natural fault planes, rather than rectangular fault segments, since triangular elements more precisely describe the curvature of faults. Figure 5 shows attribute maps of the fault plane for depth, dip, and curvature. The database for the fault plane construction, i.e., the cross sections, is largely based on interpreted geology, but it represents the best deep structural information available for that region.

3.2. Fault-Parallel Flow

[19] The hanging wall volume (i.e., that side of a nonvertical fault that occurs above it) of the fault, built up of tetrahedra and generated from the DEM, was moved along the fault plane in the direction indicated by the GPS velocities (SSE at 150°; see Figure 2), using the "fault-parallel flow" algorithm [*Egan et al.*, 1999]. In 3DMove, the hanging wall itself has to be moved along the fault plane to cause deformation within it. This is in a strict sense a reversal of the present tectonic situation, i.e., the underthrusting and wedge indentation of the Adriatic lithosphere underneath the Eastern Alps. But since relative movement is the same in both situation, the resulting deformation does not differ. Fault-parallel flow is designed to kinematically model hanging wall movements on complex faults from fold and thrust belts, where deformation is accommodated by fault-parallel shear [e.g., *Tanner et al.*, 2003]. In fault-parallel flow, particle flow is restricted to flow lines parallel to the fault surface. As each node of the tetrahedra has an individual flow path, differential movement results in internal strain and rotation of the tetrahedra. For the total displacement value we used 4 km. The upscaling to "geologic" displacement and timescales was necessary as the grid size of the fault plane was 2 km and lower displacement values would have resulted in strain fields dominated by algorithm noise. An analysis on a more detailed fault surface showed that strain maxima resulting from lower and higher slip values do not differ in their position, but localized zones of deformation become broader [*Tanner et al.*, 2006]. These results support our upscaling approach, since we focus on major, regional-scale structures.

3.3. Strain Field of the Friuli/NW Slovenia Area

[20] In the western sector we observe only one strain maximum subparallel and close to the primary fault, generated by its regular listric shape (Figure 6). In the central sector, the ramp-flat-ramp structure causes several fault-parallel strain maxima. In contrast, as in the western and central sector the influence of the fault corrugations is low, the oblique collision with both the fault corrugations and a ramp-flat-ramp structure of the eastern fault trace produces a complex strain pattern in the eastern sector revealing strain maxima striking parallel, as well as perpendicular, to the primary fault.

[21] After a slip of 4 km, the resultant maximum principal strain e_1 in the hanging wall ranges from 0 to 30% (Figure 6). The average value is 7.3%. In the western sector we observe high strain occurring as one band subparallel and close to the SW–NE trending active front. The central sector presents three bands of high strain subparallel to the W–E trending primary fault. In the eastern sector the strain pattern is more complex and reveals structures of high strain that are both parallel and perpendicular to the NW–SE trending active front. Furthermore, we analyzed the vorticity within the hanging wall (Figure 6). For steady progressive deformation the kinematic vorticity number W_k is a measure of the noncoaxial component of deformation [*Truesdell*, 1954, *Means et al.*, 1980]. Thereby, $W_k < 0.5$ signifies predominant pure shear and $W_k > 0.5$ predominant simple shear. The vorticity values in our strain analysis range from 0.24 to 0.94. The vorticity is closer to 1 in the central and eastern sector, whereas the western sector is characterized by a dominant low vorticity and therefore pure shear component.

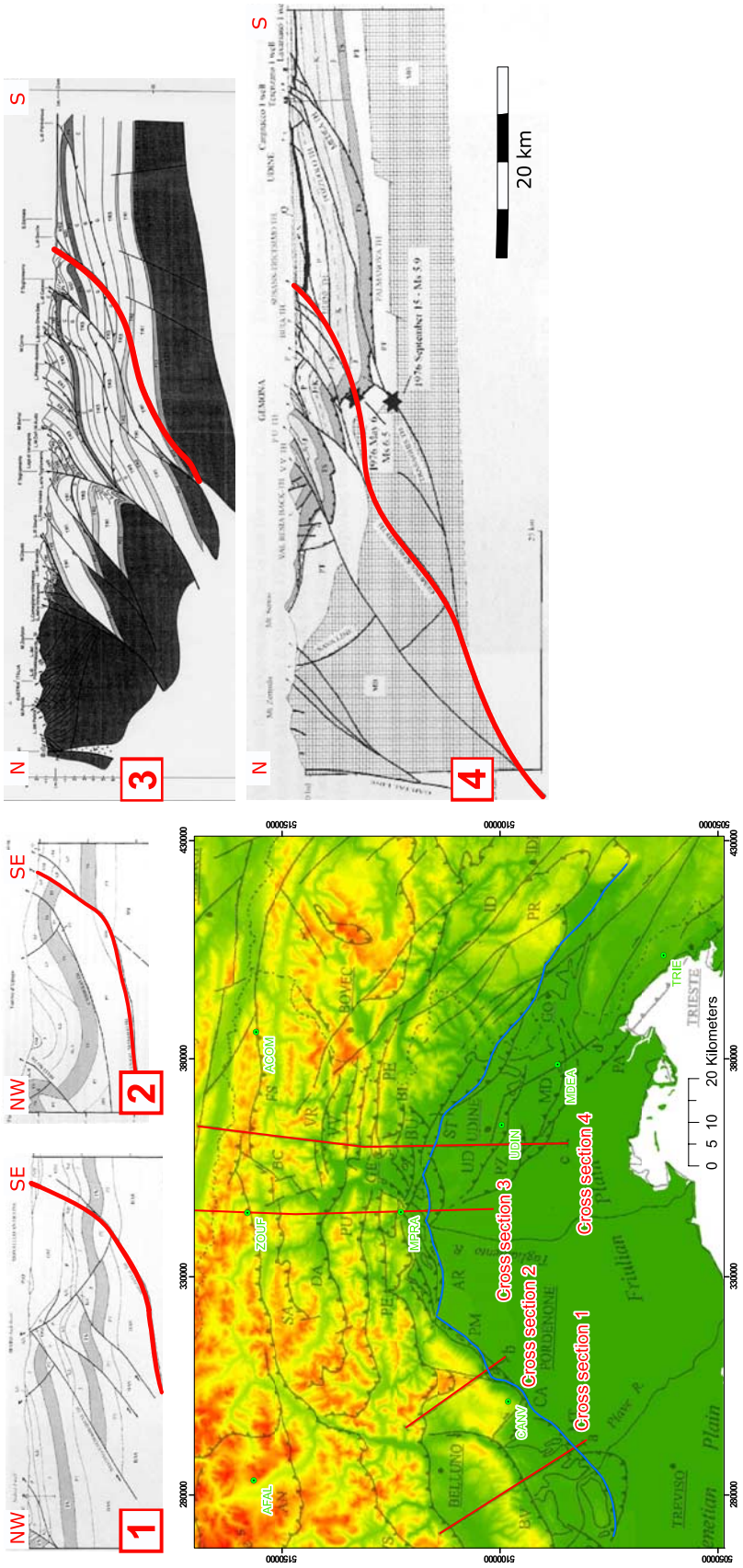

Figure 4. Digitized fault traces in (1) the structural map of *Galadini et al.* [2005] (with permission) (lower left, trace marked in blue) and (2) the four cross sections (upper left to right, trace marked in red).

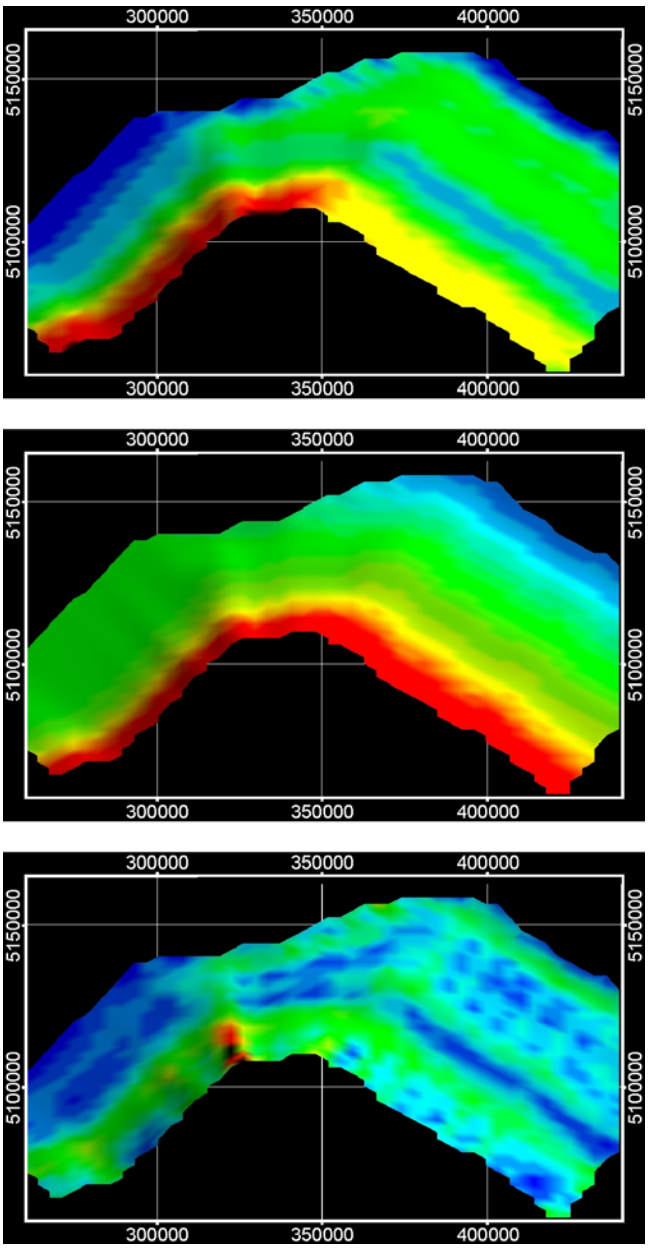

Figure 5. Fault plane attributes. Note that the fault plane is extended upward, as needed by the fault-parallel algorithm to guide the movement of the hanging wall volume. (top) Depth of the fault plane. Depth ranges from 10,000 m (extended part; red) to −30,000 m (blue). (middle) Dip of the fault plane. Dip ranges from 0 (blue) to 65° (red). (bottom) Curvature of the fault plane. Curvature ranges from 0 (blue) to 0.16 (red).

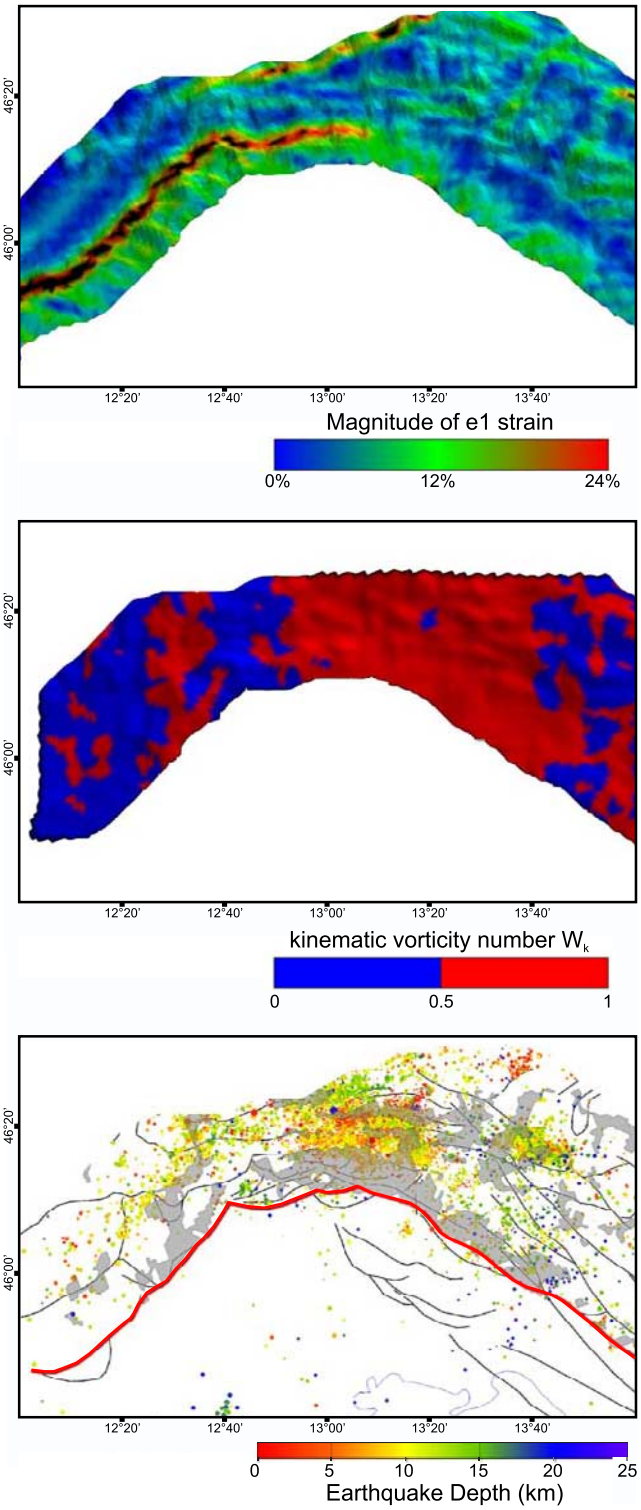

Figure 6. Hanging wall. (top) Magnitude of e_1 strain. (middle) Kinematic vorticity number W_k. (bottom) The highest probability of faulting; that is, the highest seismic hazard, is in areas of increased strain (e_1 strain magnitude >5%) and predominant simple shear (vorticity number W_k > 0.5). These areas are marked gray. Seismicity distribution and structural map are as in Figure 2. The red line represents the modeled fault trace.

3.4. Sensitivity Analysis of the Kinematic Model

[22] Movement direction and the geometry of the fault plane are the two major parameters that influence the strain distribution in the hanging wall. In the following, the effects of changes of these parameters, i.e., the sensitivity of the model, are discussed.

3.4.1. Application of Different Movement Directions

[23] The strain analysis presented in section 3 was performed for the deformation generated by the movement

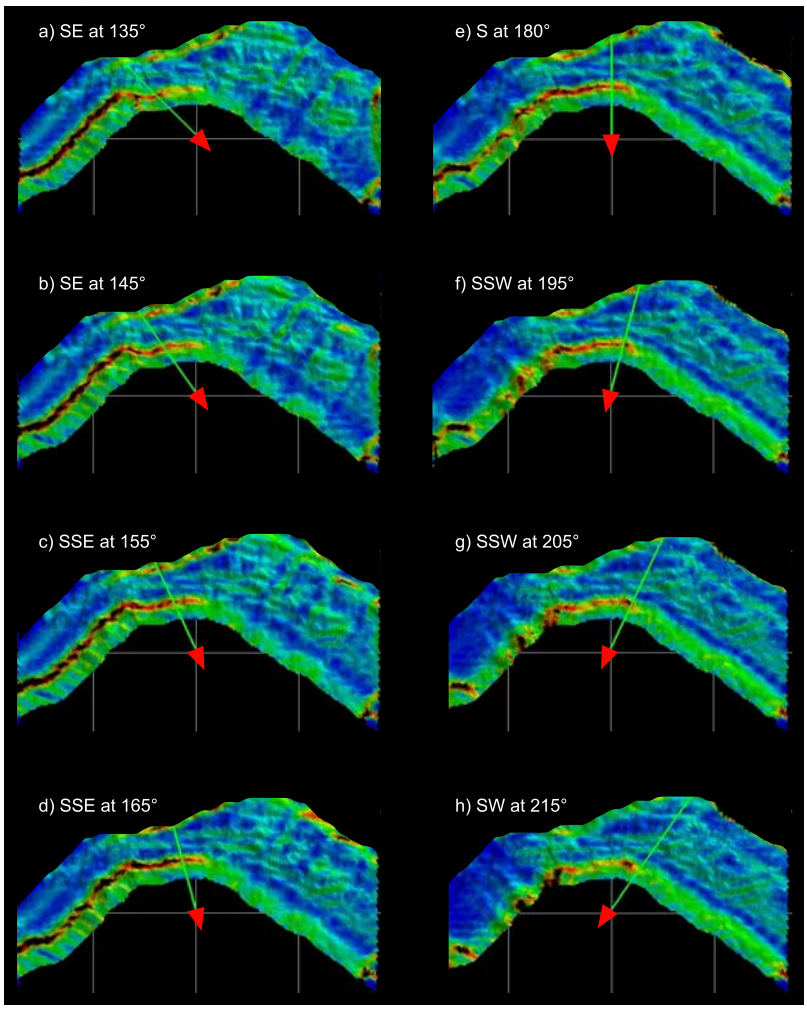

Figure 7. Magnitude of e_1 as color map as response to different movement directions (from SE (135°) to SW (215°)). Color map is as in Figure 6.

indicated by the GPS velocity field. The angle of collision (SSE at 150°) of southern Friuli (footwall) with respect to northern Friuli (hanging wall) was inferred from the solution stabilized for northern Friuli.

[24] The error ellipses of the GPS velocity vectors (see Figure 2) indicate that the actual angle of collision could vary by 10° to 20°. To test the effects of different movement directions, we moved the hanging wall along the fault plane with several different directions (from SE (135°) to SW (215°)). Figure 7 demonstrates the variation of the distribution of the e_1 strain magnitude.

[25] The strain magnitude of the western band of high strain continuously decreases from Figure 7a to 7h, i.e., from a frontal collision with the western fault trace to an oblique one. Furthermore, the band of high strain gradually loses its coherence and begins to be disrupted by areas of intermediate strain. The opposite occurs close to the eastern fault trace. An initially discontinuous band of alternating low and intermediate strain values turns into a coherent band of increased intermediate strain. In the central sector the bands of intermediate and high strain present their highest magnitude for a north directed collision. Another important change of the strain distribution occurs in the hinterland of the eastern sector, which presents the most complex strain distribution. From Figures 7a to 7h the structures of moderate strain oriented perpendicular to the strike of the fault gradually disappear, and are replaced by both fault-parallel and E–W striking structures.

[26] The detailed strain analysis applied in this study (SSE at 150°) lies between Figure 7b and 7c. The strain distributions of Figures 7a to 7d indicates that differences produced by variations of 10° to 20° with respect to the direction of this study are only minor. In this range the deformation observation is almost unchanged and the strain magnitude only differs slightly.

3.4.2. Alternative Fault Planes

[27] The fault plane used for the kinematic model of this study was built with information of the velocity field, proposed seismogenic sources, structural maps, cross sections, seismicity and DEM. The aim was to estimate the geometry of the recently active front of the foreland-propagating thrust system.

[28] Whereas in the western sector, the active front is clearly defined (see section 3.1.), the central and eastern

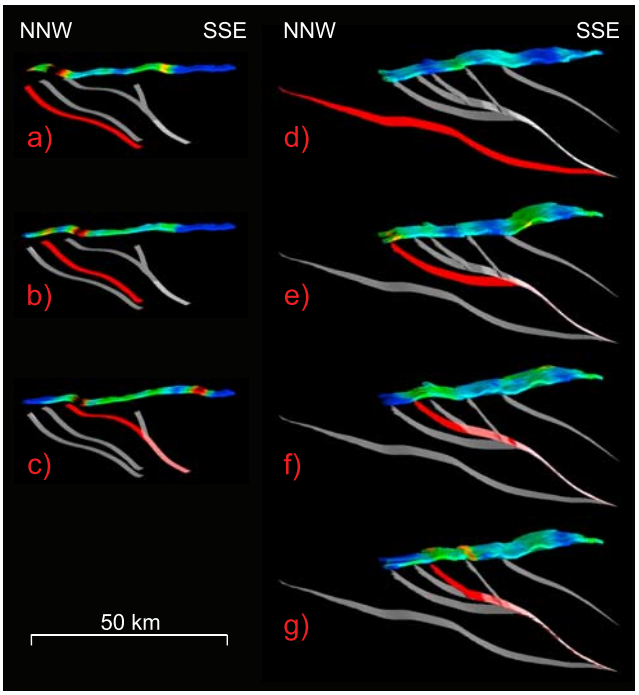

Figure 8. Two two-dimensional models with alternative fault planes. (a to c) Central sector. (d-g) Eastern sector. In each model the slip value was 4000 m and the applied direction SSE at 150°. The color map is as in Figure 6. In each plot, the fault used is marked red. Figures 8a and 8d are the fault traces used to build the recently active thrust front of this study.

sector present various faults and it is currently not known which of them represents the recently active front. To evaluate the effects of the application of alternative fault planes on the strain distribution, we created two two-dimensional models for the central and eastern sectors (Figure 8). We imported all fault traces that represent possible active structures (G. Bressan, personal communication, 2006) of the cross sections 3 and 4 (see section 3.1) into 3DMove to form two separate two-dimensional models. In each model, we moved along the three and four, respectively, southernmost faults (see Figure 8), applying the same parameters as before.

[29] The two-dimensional models show that the resultant strain moves northward when using more northerly fault planes. But the resultant strain patterns are very similar. The models 2b, 2c and 2d all have two major strain maxima produced by the ramp-flat-ramp structure the three faults have in common. The surface fault trace applied in model 2a is located south of all FReDNet GPS stations. Therefore, there is no kinematic evidence that this fault represents a possible, recently active structure. The strain distribution of the models 1a, 1b and 1c are also comparable. One major strain maxima is located close to the fault and followed by a rather distributed strain field with several minor maxima.

[30] With the criteria presented in section 3.1, the fault plane of this study represented the best alternative to estimate the recently active thrust front. The two-dimensional models show that even if we chose an alternative fault trace, no major changes in the strain pattern would be expected, but only a northward shift of the whole strain field.

4. Discussion

4.1. Interpretation of Friulian CGPS Velocities

[31] The resultant GPS velocity field constrains the area in which the horizontal shortening of approximately 2 mm/a takes place (Figure 2). The southern border is defined by the stations UDIN, MDEA and TRIE, which present crustal velocities that are in the range of those estimated for Adria [e.g., *D'Agostino et al.*, 2005]. The stations ACOM, ZOUF and AFAL define the northern border of the shortening sector. These stations are north of the active seismicity and demonstrate only a residual northward movement of about 1 mm/a with respect to stable Eurasia. As AFAL, ZOUF, ACOM and MPRA, also CANV is situated north of the active thrust front. Thus, the long-term geologic (block) velocity at CANV should be significantly lower than the one of the Adriatic microplate. But the geodetically determined velocity of CANV shows the opposite. CANV does not move slower, but with an even slightly higher velocity than Adria. Whether this anomalous high velocity of CANV is really based on crustal kinematics, may be related to its vicinity to the SE verging, active Polcenigo-Maniago Thrust (PMT) (1873 (M > 6) earthquake) [*Galadini et al.*, 2005], or affected by monument instabilities is not discussed in detail here. A prolonged time series that significantly exceeds the minimum time span of 2.5 years is needed and will provide a better basis for interpreting a single anomalous site velocity.

4.2. Interpretation of the Kinematically Modeled Strain Field

[32] The software package 3DMove is able to move three-dimensional objects over faults, using appropriate kinematic algorithms. The algorithms bind the deformation of the faulted objects to the fault morphology, while maintaining a structural continuum. Since this a kinematic geometric modeling program, it is not possible to add rheological information to the various geological bodies. In addition, objects can only be moved upon one fault at one time. 3DMove is based on the pure geometric approach normally used to retrodeform geologic models, while maintaining structural continuity, bed length and volume, etc as constrains. In its simplest form, this involves two-dimensional models with downdip movement. In our study, we use the same techniques, but for a three-dimensional model with a curved and regionally convolute fault morphology, and move the hanging wall obliquely (according to the GPS data). In essence, the models produced by 3DMove can thus demonstrate the far-field effect of fault movement, as caused by the kinematic movement of the geologic objects over the fault morphology.

[33] Our kinematic model show the effects of the indenter-shaped active fault front on the development of secondary fault systems. Because of sparse information on the active front, the proposed fault plane is a simplified approximation of the real plate boundary between the Adriatic microplate and Europe. But on the basis of a sensitivity analysis (testing of alternative fault planes, application of different movement directions that lie in the range of the

estimated error, application of different slip values; see section 3.4), we find that the principal strain results, i.e., the pattern of zones of the highest probability of faulting, do not change significantly. The modeled strain field is of pure kinematic origin, produced by the movement along the fault. The three-dimensional geologic restoration algorithms and tools of 3DMove are based on the pure geometrical approach. Thus, the deformation of the hanging wall is only controlled by the interaction of the movement direction, the total slip and the fault geometry. In general, higher strain is concentrated at zones of high fault curvature. The modeled fault plane of this study presents three types of curvature: (1) change of fault dip, obtained from the cross sections; (2) fault corrugations (generated by curvature of the surface fault trace), and (3) the general indenter-shaped geometry, i.e., the related segment linkages between the western, central and eastern sector.

[34] The orientation of the movement direction determines whether the effect of one curvature type on the strain distribution is strong or weak. The oblique collision of Adria with eastern southern Alps causes a predominant frontal, perpendicular collision with the active front in the western and central sector, whereas in the eastern sector the movement direction forms a relatively acute angle (30°) with the fault front. As a consequence each sector has its individual strain field (Figure 6). In the western sector, the single band of high strain is generated by the regular listric shape of the primary fault. In the central sector, the primary fault presents a ramp-flat-ramp structure and causes several fault-parallel strain maxima. In contrast, in the western and central sector the influence of the fault corrugations is low, the oblique collision with both the fault corrugations and a ramp-flat-ramp structure of the eastern fault trace produces a complex strain pattern in the eastern sector revealing strain maxima striking parallel, as well as perpendicular, to the primary fault.

[35] We consider the absolute strain magnitude to be the main factor controlling whether a rupture occurs or not. Deformation nucleates at strain maxima. Therefore, for example, the strain distribution around faults can be directly correlated to the density of fractures [*Okubo and Schultz*, 2005]. On a regional scale, the fault slip induced, secondary structures will be faults. It is along these structures that regional elastic distortions are minimized by displacement (earthquakes). Another important factor is the amount of vorticity. It determines whether a rupture occurs in a certain area or the energy is transferred to the neighborhood. The higher vorticity values in the central and northern part of the eastern sector (Figure 6) are mainly caused by the shape of the indenter fault. The hanging wall bodies try to flow around the apex of the indenter and thereby obtain a rotational component.

[36] When trying to correlate modeling results from the Friuli area with the seismicity distribution monitored since 1977, one should bear in mind that in this area the typical recurrence intervals of earthquakes $M > 6$ are 1 order of magnitude longer than the 30 year long history of seismic monitoring. The stress redistribution caused by the 1976 sequence possibly produced a maximum seismic activity in the central sector. But it cannot be assured that to the east and west the seismic activity reaches the same level within the next 100 or 200 years. Therefore, it is probably misleading to tune model parameters in order to obtain the best fit with the seismic energy recently released from 1977 until today, as for example done by *Rossi et al.* [2005]. Rather modeling results should help to predict active structures that have been inactive, i.e., accumulating strain, during the last three decades.

[37] We defined the concurrence of high strain (e_1 strain magnitude >5%) and high vorticity ($W_k > 0.5$), as zones of high probability of faulting (Figure 6). A comparison of the distribution of these zones with proposed seismogenic sources and the observed seismicity since 1977 is interesting. In the western sector, zones of highest probability of faulting are consistent with the observed seismicity and proposed seismogenic sources. The western sector is mainly characterized by one active front, whereas in the central sector two or three subparallel faults interact. The eastern sector is more complex. Within the area of seismicity there is only one proposed seismogenic source, the one responsible for the 1998 Bovec earthquake. But the broad belt of seismicity cannot be explained by this fault only. Our model suggests an additional set of SW–NE trending faults in that region. Because these faults are absent on structural maps, we analyzed in detail the seismicity of that area. We focused on several larger events and their related aftershocks. A three-dimensional view of these events as well as the top view show a vertical, SW–NW trending distribution (Figure 9). The vertical distribution strongly indicates strike-slip faulting. It seems that the eastern sector, comprising east Friuli and NW Slovenia, is characterized by two sets of strike-slip faults oriented subperpendicular to each other; a situation similar to the one observed by *Tapponnier et al.* [1982] in their analogue indenter model of the Himalayan tectonics. They recognized two sets of strike-slip faults, one characterized by sinistral movement subperpendicular to the right indenter side and guiding the extrusion, the other oriented subparallel to the right indenter side with dextral movement. The orientation of the fault-parallel set correlate with the dextral strike-slip fault related to the 1998 Bovec earthquake [e.g., *Galadini et al.*, 2005]. The fact that the fault-perpendicular structures have not yet been mapped at the surface in Friuli could signify that the structures are either blind or very young and less developed than the structures of the Dinaric paleofault system. Two of five aftershock alignments do not reach the surface; a possible indication of blind faulting.

5. Summary and Conclusions

[38] The Friuli GPS velocity field obtained from GPS measurements defines an area that is characterized by 1.6 to 2.2 mm/a of shortening. Furthermore, it indicates an oblique collision, with southern Friuli moving NNW (at 330°) toward northern Friuli. The shortening rate and movement direction of southern Friuli/northern Adria is consistent with geomorphologic studies along the Montello Thrust, as well as former published GPS velocity fields. But since our analysis spans longer time series and includes more local GPS sites (first complete processing of FReDNet), it presents more details in the region of interest.

[39] Our modeling results demonstrate that the combination of geodetic crustal velocities and kinematic modeling can contribute to the understanding of the active tectonics in the Friuli area. A three-dimensional model of the oblique

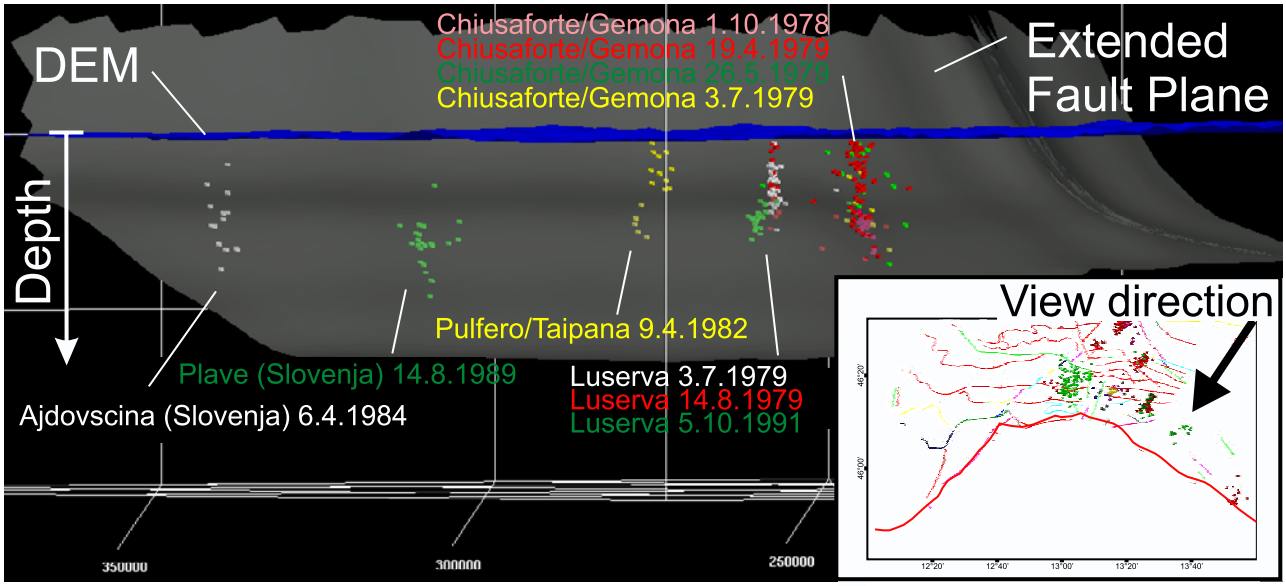

Figure 9. Three-dimensional view, perpendicular to the eastern fault trace. View from NE. Gray, fault plane; blue, DEM. The events that present a SW–NE trending alignment are shown. Each aftershock sequence is represented by one color. Inset shows the top view; view direction is indicated.

collision of the Adriatic microplate with the eastern southern Alps, guided by the indenter-shaped fault plane, is consistent with the current knowledge on seismogenic sources, but also indicates fault systems that may have not been recognized yet. The strain field induced by moving on the recently active front of the foreland-propagating thrust system indicates active, secondary structures in the hanging wall. Thereby, the concurrence of a high strain magnitude and a high vorticity number signifies a high probability of faulting. In the western sector, zones of the highest probability of faulting are scarce and mainly show one, discontinuous, fault-parallel structure. The central sector, i.e., the area of Tagliamento River, presents three fault-parallel structures that are consistent with the interaction of three active thrusts proposed by *Galadini et al.* [2005]. The strain field of the eastern sector indicates intense secondary faulting in the hinterland. Two sets of faults oriented subperpendicular to each other interact in this sector. The orientation of the fault-parallel set correlate with the dextral strike-slip fault related to the 1998 Bovec earthquake. The fault-perpendicular structures are absent in structural maps, but can be correlated with selected seismic events and related aftershocks and indicate sinistral strike-slip faulting. The situation of two interacting strike-slip faults is similar to the one analyzed by *Tapponnier et al.* [1982] in their analogue indenter model of the Himalayan tectonics.

[40] **Acknowledgments.** D. I. Nikolayev wrote the code used to compute the vorticity. B. King (MIT) and T. A. Herring (MIT) provided a number of helpful suggestions for the GPS data processing. Thanks also to G. Bressan for providing geological cross sections and E. Serpelloni for discussing our GPS and modeling approach at the beginning. Comments by R. Bennett and an anonymous reviewer greatly helped to improve the manuscript.

References

Altamimi, Z., P. Sillard, and C. Boucher (2002), ITRF2000: A new release of the International Terrestrial Reference Frame for earth science applications, *J. Geophys. Res.*, *107*(B10), 2214, doi:10.1029/2001JB000561.

Anderson, H. A., and J. A. Jackson (1987), Active tectonics of the Adriatic region, *Geophys. J. R. Astron. Soc.*, *91*, 937–983.

Battaglia, M., M. H. Murray, E. Serpelloni, and R. Bürgmann (2004), The Adriatic region: An independent microplate within the Africa-Eurasia collision zone, *Geophys. Res. Lett.*, *31*, L09605, doi:10.1029/2004GL019723.

Bechtold, M. (2007), Earthquake Potential in the Italian southern Alps, M.S. thesis, 138 pp., Univ. of Göttingen, Göttingen, Germany.

Benedetti, L., P. Tapponnier, G. C. P. King, B. Meyer, and I. Manighetti (2000), Growth folding and active thrusting in the Montello region, Veneto, northern Italy, *J. Geophys. Res.*, *105*(B1), 739–766.

Blewitt, G., and D. Lavallée (2002), Effect of annual signals on geodetic velocity, *J. Geophys. Res.*, *107*(B7), 2145, doi:10.1029/2001JB000570.

Bressan, G., A. Snidarcig, and C. Venturini (1998), Present state of tectonic stress of the Friuli area (eastern southern Alps), *Tectonophysics*, *292*, 211–227, doi:10.1016/S0040-1951(98)00065-1.

Bressan, G., P. L. Bragato, and C. Venturini (2003), Stress and strain tensors based on focal mechanisms in the seismotectonic framework of the Friuli-Venezia Giulia region (northeastern Italy), *Bull. Seismol. Soc. Am.*, *93*(3), 1280–1297, doi:10.1785/0120020058.

Caporali, A., et al. (2008), Geokinematics of central Europe: New insights from the CERGOP-2/Environment Project, *J. Geodyn.*, *45*, 246–256, doi:10.1016/j.jog.2008.01.004.

Carulli, G. B., and M. Ponton (1992), Interpretazione strutturale profonda del settore centrale carnico-friulano, *Studi Geol. Camerti*, vol. spec. 2, 275–284.

Castellarin, A., R. Nicolich, R. Fantoni, L. Cantelli, M. Sella, and L. Selli (2006), Structure of the lithosphere beneath the Eastern Alps (southern sector of the TRANSALP transect), *Tectonophysics*, *414*, 259–282, doi:10.1016/j.tecto.2005.10.013.

D'Agostino, N., D. Cheloni, S. Mantenuto, G. Selvaggi, A. Michelini, and D. Zuliani (2005), Strain accumulation in the southern Alps (NE Italy) and deformation at the northeastern boundary of Adria observed by CGPS measurements, *Geophys. Res. Lett.*, *32*, L19306, doi:10.1029/2005GL024266.

Egan, S. S., S. Kane, T. S. Buddin, G. D. Williams, and D. Hodgetts (1999), Computer modelling and visualisation of the structural deformation caused by movement along geological faults, *Comput. Geosci.*, *25*, doi:10.1016/S0098-3004(98)00125-3.

Fantoni, R., C. Barbieri, D. Catellani, D. Castellarin, A. Di Giulio, and C. Pessina (2001), The record of south-Alpine events in the Venetian foreland and foredeep, *Geol. Palaontol. Mitt. Innsbruck*, *25*, 79–81.

Feigl, K. L., et al. (1993), Space geodetic measurement of crustal deformation in central and southern California, 1984–1992, *J. Geophys. Res.*, *98*(B12), 21,677–21,712.

Galadini, F., M. E. Poli, and A. Zanferrari (2005), Seismogenic sources potentially responsible for earthquakes with M > 6 in the eastern southern

Alps (Thiene-Udine sector, NE Italy), *Geophys. J. Int.*, *161*(3), 739–762, doi:10.1111/j.1365-246X.2005.02571.x.

Grenerczy, G., G. Sella, S. Stein, and A. Kenyeres (2005), Tectonic implications of the GPS velocity field in the northern Adriatic region, *Geophys. Res. Lett.*, *32*, L16311, doi:10.1029/2005GL022947.

Herring, T. A. (2003a), GLOBK: Global Kalman filter VLBI and GPS analysis program, version 10.1, 91 pp., Mass. Inst. of Technol., Cambridge.

Herring, T. A. (2003b), MATLAB Tools for viewing GPS velocities and time series, *GPS Solutions*, *7*(3), 194–199.

McClusky, S., et al. (2000), Global Positioning System constraints on plate kinematics and dynamics in the eastern Mediterranean and Caucasus, *J. Geophys. Res.*, *105*(B3), 5695–5720.

Means, W. D., B. E. Hobbs, G. S. Lister, and P. F. Williams (1980), Vorticity and non-coaxiality in progressive deformations, *J. Struct. Geol.*, *2*(3), 371–378.

Okubo, C. H., and R. A. Schultz (2005), Evolution of damage zone geometry and intensity in porous sandstone: Insight gained from strain energy density, *J. Geol. Soc.*, *162*(6), 939–949, doi:10.1144/0016-764904-148.

Peruzza, L., M. E. Poli, A. Rebez, G. Renner, S. Rogledi, D. Slejko, and A. Zanferrari (2002), The 1976–1977 seismic sequence in Friuli: New seismotectonic aspects, *Mem. Soc. Geol. Ital.*, *57*, 391–400.

Pfiffner, O. A., and J. G. Ramsay (1982), Constraints on geological strain rates: Arguments from finite strain states of naturally deformed rocks, *J. Geophys. Res.*, *87*(B1), 311–321.

Poli, M. E., and G. Renner (2004), Normal focal mechanisms in the Julian Alps and Prealps: seismotectonic implications for the Italian-Slovenian border region, *Boll. Geofis. Teorica Appl.*, *45*(1–2), 51–69.

Poli, M. E., L. Peruzza, A. Rebez, G. Renner, D. Slejko, and A. Zanferrari (2002), New seismotectonic evidence from the analysis of the 1976–1977 and 1977–1999 seismicity in Friuli (NE Italy), *Boll. Geofis. Teorica Appl.*, *43*, 53–78.

Reilinger, R., et al. (2006), GPS constraints on continental deformation in the Africa-Arabia-Eurasia continental collision zone and implications for the dynamics of plate interactions, *J. Geophys. Res.*, *111*, B05411, doi:10.1029/2005JB004051.

Rossi, G., C. Ebblin, and M. Zadro (2005), 3D finite-elements kinematic model of the Adria northern region: Stress analysis, *Boll. Geofis. Teorica Appl.*, *46*(1), 23–46.

Serpelloni, E., G. Vannucci, S. Pondrelli, A. Argnani, G. Casula, M. Anzidei, P. Baldi, and P. Gasperini (2007), Kinematics of the western Africa-Eurasia plate boundary from focal mechanisms and GPS data, *Geophys. J. Int.*, *169*(3), 1180–1200, doi:10.1111/j.1365-246X.2007.03367.x.

Slejko, D., G. Neri, I. Orozova, G. Renner, and M. Wyss (1999), Stress field in Friuli (NE Italy) from fault plane solutions of activity following the 1976 main shock, *Bull. Seismol. Soc. Am.*, *89*(4), 1037–1052.

Tanner, D. C., J. H. Behrmann, and H. Dresmann (2003), Three-dimensional retro-deformation of the Lechtal Nappe, northern Calcareous Alps, *J. Struct. Geol.*, *25*, 737–748, doi:10.1016/S0191-8141(02)00057-3.

Tanner, D. C., T. Lohr, C. M. Krawczyk, O. Oncken, H. Endres, R. Samiee, H. Trappe, and P. Kukla (2006), Multi-scale structures around faults—Comparison of natural and 3D kinematic retrodeformation modelling data from Permian strata in the NW German Basin, paper presented at GV International Conference, Geol. Ver., Potsdam, Germany, 25–29 Sept.

Tapponnier, P., G. Peltzer, A. Y. Le Dain, R. Armijo, and P. Cobbold (1982), Propagating extrusion tectonics in Asia: New insights from simple experiments with plasticine, *Geology*, *10*, 611–616.

Truesdell, C. (1954), *The Kinematics of Vorticity*, 232 pp., Indiana Univ. Press, Bloomington.

M. Battaglia, Department of Earth Sciences, University of Rome I "La Sapienza," Piazzale Aldo Moro 5, I-00185 Roma, Italy.

M. Bechtold, Institute of Chemistry and Dynamics of the Geosphere, Institute Agrosphere, Research Centre Jülich, D-52425 Jülich, Germany. (m.bechtold@fz-juelich.de)

D. C. Tanner, Leibniz Institute for Applied Geosciences, Stilleweg 2, D-30655 Hannover, Germany.

D. Zuliani, Centro Ricerche Sismologiche, Via Treviso 55, I-33100 Udine, Italy.